Stress dependence of the critical currents in neutron irradiated (RE)BCO coated conductors

J Emhofer, M Eisterer, and H W Weber

Atominstitut, Vienna University of Technology, Stadionallee 2, 1020 Vienna, Austria

E-mail: `eisterer@ati.ac.at`

Abstract. The application of HTS coated conductors in future fusion or accelerator magnets is currently of increasing interest. High Lorentz forces and therefore high hoop stresses act on the conductors in large coils. The conductor is furthermore exposed to neutron radiation in fusion or accelerator magnets. The expected neutron fluence over the desired lifetime of such magnets can be simulated by irradiation experiments in a fission reactor. The coated conductors were characterized in the pristine state and after irradiation to a fast neutron fluence of $1 \times 10^{22} \, \mathrm{m}^{-2}$ (ITER design fluence). The sensitivity of the critical currents to applied stress was measured in liquid nitrogen. The cold part of the set-up was positioned between a rotatable split coil electro-magnet for assessing the I_c-anisotropy up to $1.4 \, \mathrm{T}$ under maximum Lorentz force configuration.

The I_c-sensitivity to applied stress changed significantly in the GdBCO/IBAD-conductors after irradiation, whereas nearly no change was observed in the YBCO/RABiTS-conductor. Furthermore, I_c and T_c were strongly reduced in the GdBCO/IBAD-sample after irradiation. The angular dependence of I_c changed for both samples in different ways after the irradiation, but no change in the angular dependence was observed upon applying stress.

The high neutron capture cross-section of Gd and the resulting strong reduction of T_c seem to be responsible for the different stress dependence of I_c in irradiated Gd-123 coated conductors.

1. Introduction

Impressive progress in coated conductor development has been made in recent years [1]- [3]. The possibility of using liquid nitrogen as the coolant, the high mechanical stability [4]-[10] and the robustness of YBCO coated conductors against neutron irradiation [11][12] render YBCO coated conductors promising candidates for applications in future fusion or accelerator magnets. Tensile stress or strain affect the performance of the conductors reversibly up to the irreversible stress/strain limit (σ_{irr} / $\varepsilon_{\mathrm{irr}}$). In the case of Bi-2223 conductors the stress-dependence of I_c was entirely explained by the pressure dependence of T_c [13]. However, since the pressure dependence of T_c is highly anisotropic in YBCO [14], the manufacturing method and in particular the alignment of the unit-cells strongly affect the stress dependence of I_c in YBCO. Recent studies [13][4] demonstrated that the reversible stress/strain-effects in YBCO/MOCVD and DyBCO/ISD conductors are also determined by the uni-axial pressure dependence of T_c. Furthermore, a strong field dependence of the I_c sensitivity on the applied tensile and/or compressive strain was found for YBCO/IBAD/MOCVD [4][5][8], YBCO/RABiTS/MOD [6][7] and YBCO/MOCVD/PLD/IBAD [10] samples.

The change in I_c caused by neutron radiation depends on the superconducting material, the neutron energy, magnetic field and temperature. Fast neutrons ($E > 0.1\,\mathrm{MeV}$) generate collision cascades in cuprates by transferring sufficient energy to a primary knock-on atom, which initiates further collisions [15][16]. These collisions lead to local melting of the lattice and the formation of spherical defects with a diameter of $\approx 6\,\mathrm{nm}$ [15]. The size of these normal conducting impurities matches the size of a flux line core ($2\xi_{a,b} \approx 6\,\mathrm{nm}$ at $77\,\mathrm{K}$) and is, therefore, optimal for flux pinning. Furthermore, these defects are uncorrelated and randomly distributed. Fast-neutron-induced cascades have been shown to be responsible for flux pinning and intra-grain critical current enhancement in (RE)BCO [17][15].

Thermal and epi-thermal neutrons do not lead to extended defects in YBCO. Epi-thermal neutrons (in the keV range) may create point defects or clusters, if the recoil energy of the primary knock-on atom is high enough to displace at least one atom. These point defects disturb the regularity of the CuO_2 planes,[18], which reduces the critical temperature. The reduction in T_c is rather weak in YBCO (about -2 K for a fast neutron fluence $\Phi \cdot t = 10^{22}\,\mathrm{m}^{-2}$ [11], where Φ and t denote the fast neutron flux density and the irradiation time, respectively). Thermal neutrons ($E < 0.5\,\mathrm{eV}$) do not affect the material by direct collisions, as the energy transferred by elastic collisions is below the displacement energy of a single atom. The neutron capture cross is negligible in YBCO.

Nuclei with high neutron capture cross-sections $\sigma(n, \gamma)$ should be avoided when the materials have to be exposed to neutron irradiation. Unfortunately, state-of-the-art (RE)BCO coated conductors contain gadolinium (GdBCO) or samarium (SmBCO) having high neutron capture cross-sections. The thermal neutron capture cross-sections of the two stable isotopes $^{155}\mathrm{Gd}$ and $^{157}\mathrm{Gd}$ with a natural abundance of 14.8% and

15.7%, respectively, are as high as 6.074×10^4 b and 2.537×10^5 b, respectively [19]. (One barn, b, corresponds to $10^{-28}\,m^2$.) After capturing a neutron, the excited nucleus emits γ-rays and the corresponding recoil energy is transferred to the nucleus. This recoil is sufficiently high to displace the excited ^{156}Gd and ^{158}Gd nuclei thus creating a point defect. Neglecting the kinetic energy of the neutron, the recoil energy was calculated to be 29 eV and 34 eV for the excited ^{156}Gd and ^{158}Gd nuclei [17]. Hence, in Gd or Sm-compounds the thermal and epi-thermal neutrons of the TRIGA reactor spectrum play a crucial role and should be removed for the simulation of a fusion spectrum by a fission reactor, since the expected fluence of low energy neutrons is very small at the magnet location of a fusion device.

The results reported in this work refer to GdBCO/IBAD and YBCO/RABiTS conductors irradiated with the entire neutron energy spectrum of the TRIGA reactor [20].

2. Samples

Two different (RE)BCO coated conductors were used for this study. The SuperPower SCS4050 tape, which consists of a $GdBa_2Cu_3O_{7-\delta}$ (GdBCO) superconducting layer on an IBAD (Ion Beam Assisted Deposition) template and the AMSC 344C (Amperium) tape consisting of an $YBa_2Cu_3O_{7-\delta}$ (YBCO) superconductor on a RABiTS (Rolling Assisted Bi-axially Textured Substrate) template.

The GdBCO layer in the GdBCO/IBAD sample was grown by MOCVD (Metal Organic Chemical Vapour Deposition) on a Hastelloy substrate with a thickness of $50\,\mu$m. On top of the GdBCO-layer a $2\,\mu$m silver layer was deposited and the entire sample was surrounded by $20\,\mu$m copper. The individual samples were 50 mm long, 4.04 mm wide and 0.1 mm thick.

The *RE*BCO layer in the YBCO/RABiTS contains yttrium and dysprosium with a nominal composition of Y:Dy:Ba:Cu of 1:0.5:2:3. The tape was grown by MOD (Metal Organic Deposition) onto a sputtered buffer stack. The cold worked and annealed (RABiTS) substrate of this tape was a $75\,\mu$m thick Ni-5 at% W alloy. A $\sim 2\,\mu$m silver layer was deposited on top of the YBCO layer and the entire tape laminated with a copper foil for better handling and stabilization. The samples were 50 mm long, 4.4 mm wide and 0.21 mm thick.

Note that different samples were used for the characterization in the pristine and the irradiated state, marked by #1 and #2 in the figures, respectively. Both samples were cut from the same spool and the self-field I_c at 77 K as well as the homogeneity of the #2-samples were checked before the irradiation by four point measurements and magnetoscans, respectively. As the YBCO/RABiTS#2 was irreversibly damaged before reaching the irreversibility limits, a third YBCO/RABiTS sample denoted by #3 was used exclusively for a self-field I_c measurement in the unirradiated state. Furthermore, shorter reference samples of 26 mm length from the same spools were irradiated in the same capsule for measurements of the irreversibility line.

3. Experimental Details

3.1. Tensile stress set-up

The cold part of our tensile stress insert (E in figure 1) was positioned between a rotatable split coil electro-magnet. Horizontal fields of up to 1.4 T can be applied at different orientations (Θ). The angular range assessed in our experiments was about 220°, including both a,b-peaks, in angular steps of 1° around $H\|c$ and $H\|a,b$ and 3° elsewhere. The cold part was immersed in liquid nitrogen during the measurements.
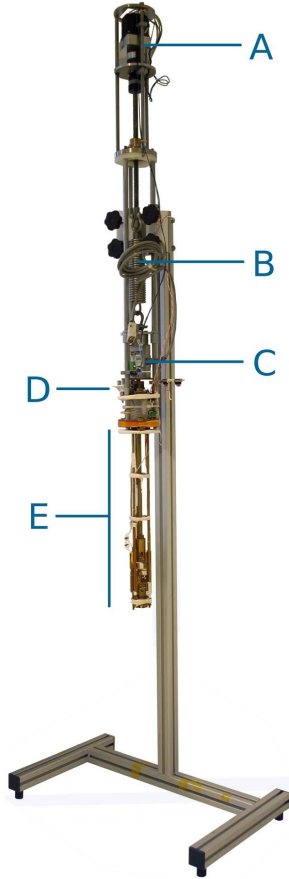
Figure 1. Photograph of the tensile stress insert. (A) Stepper motor, (B) removable spring, (C) load cell, (D) connections, heating resistor, thermal switch, safety spring, etc., (E) cold part.

The temperature variation of liquid nitrogen due to changes of ambient pressure or oxygen pick-up induces some scatter in the data. To reduce this error to an acceptable level, all data were discarded whenever the temperature at the sample position was not within 77.4±0.3 K during the measurement.

Tensile forces were set with a stepper motor (A in figure 1). A trapezoidal thread transformed the rotation to a translation along the pull rod axes. The force was transduced to the pull rod (B in figure 2) by a 1000 kN spring (B in figure 1) and a

ball bearing prevents the lower parts from rotating. A 2000 kN load cell (C in figure 1) located between the ball bearing and the pull rod, measured the applied force.
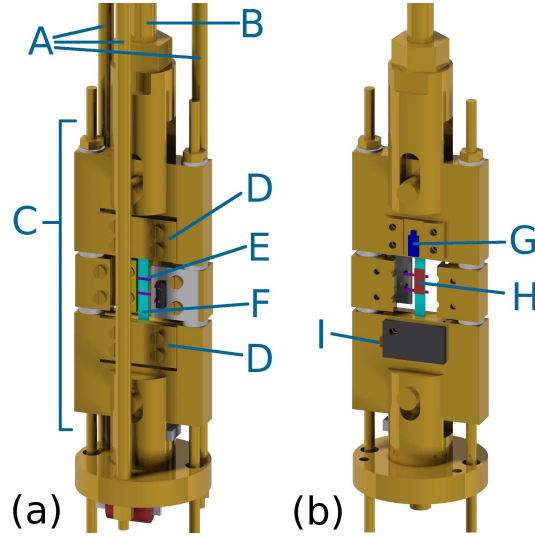
Figure 2. CAD-drawings of the lower cold part of the set up. The front side is illustrated in (a) whereas the back side, without the push rods and with an artificial cut-out in the centre, is illustrated in (b). Wires and cables are not depicted. (A) Push rods, (B) pull rod, (C) removable carriage, (D) current clamps, (E) voltage contacts, (F) coated conductor, (G) Hall probe, (H) strain gauge, (I) reference strain gauge on a stress-free reference coated conductor.

Figure 2 shows the front and back side of the cold part. The coated conductor (F in figure 2) is clamped between the upper and the lower part of the removable carriage (C in figure 2). The pull and the push rods also act as current bars and therefore brass was used for the cold part. The upper and lower parts of the removable carriage are insulated from each other by Teflon inserts. A Pt100-Class 1/5 sensor was used to monitor the temperature close to the sample.

The voltage contacts (E in figure 2) were glued with silver paste, allowing small position rearrangements due to elongation. The average distance between the contacts was 5 mm and I_c was evaluated using a $1\,\mu$V/cm criterion by fitting the data by a power law ($E = E_c \left(I/I_c\right)^n$, least squares method).

A strain gauge was glued directly onto the coated conductor with epoxy resin (H in fig. 2), measuring the strain of the sample. A reference strain gauge was mounted close to the sample (I in figure 2) on a small stress free coated conductor of the same type as the measured sample in order to subtract the strain caused by cooling the sample to liquid nitrogen temperatures. Both strain gauges were connected to a tunable Wheatstone bridge.

A Hall probe was mounted parallel to the tape surface in order to measure the orientation of the applied magnetic field, which was set by rotating the split coil with a stepper motor.

The full I_c-anisotropy characterization at a fixed applied force was done during one measurement cycle. Such a cycle started by increasing the force stepwise from the relaxed state to the desired force. At each step, the self-field I_c was measured. Between each step, the stress was released and I_c was re-measured. The dependence of the self-field I_c on the stress/strain was obtained from these measurements. The anisotropy measurements started after reaching the desired set-force. Angular resolved I_c-measurements were performed at 0.1 T, 0.2 T, 0.4 T, 0.6 T, 1 T and 1.4 T. After the last measurement, the computer program started the warm-up process. Typically, anisotropy measurements were performed at nine different forces, leading to a net measurement time of typically around 400 hours for one sample including periods of heating to room temperature. Note, that in the "relaxed" state a force of 10 N (11 MPa in YBCO/RABiTS and 25 MPa in GdBCO/IBAD) was applied to the samples.

3.2. Neutron irradiation

The samples were irradiated in the central irradiation facility of the TRIGA Mark II research reactor in Vienna to a fast neutron fluence of $\Phi \cdot t = 1 \times 10^{22}\,\mathrm{m^{-2}}$ ($E > 0.1\,\mathrm{MeV}$). The samples were sealed in a quartz tube and the temperature did not exceed 70° C during the irradiation. The introduced defect structure in single-crystalline YBCO was already studied in detail [21] and further irradiation studies of coated conductors can be found in [12].

3.3. Magnetoscan

The homogeneity of the superconducting layer was checked by magnetoscan imaging before and after applying the maximum tensile stress. A detailed description of the set-up can be found in [22]. The local magnetic field detected slightly above the sample but below a permanent magnet is closely related to the local current density and, therefore, provides evidence for the local quality of the sample [23].

4. Results and Discussion

4.1. Stress - strain dependence

The irradiated YBCO/RABiTS sample (figure 3) was stressed up to the irreversible limits σ_{irr} =410 MPa and ε_{irr} =0.52%. The yield strength of the substrate was reported to be 260 MPa [24] at 76 K which corresponds to a stress of 84 MPa in the YBCO/RABiTS tape. The applied stress led to a distinct irreversible deformation at the strain gauge position after applying 346 MPa (cf. figure 3). A reduction of the irreversible deformations was always observed after heating the sample to room temperature.

The Young's modulus (e) was evaluated by fitting the data between 20 N (22 MPa in YBCO/RABiTS and 50 MPa in GdBCO/IBAD) and the maximum applied stress
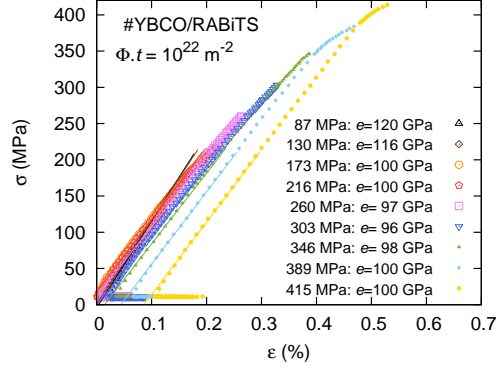
Figure 3. Stress-strain dependence of the irradiated YBCO/RABiTS sample. Different symbols denote different maximum applied stresses.

of the previous measurement loop (e.g. 173 MPa for the 216 MPa measurement). The values found for the irradiated YBCO/RABiTS sample are quoted in figure 3.

No change of Young's modulus was observed in the YBCO/RABiTS tape after irradiation, but a slight decrease by 24 GPa was observed in the GdBCO/IBAD conductor. Since these results represent the first measurements ever on irradiated GdBCO/IBAD coated conductors and in view of the lack of sufficient statistics, further experiments will be needed for confirmation. The presently available average values of the Young's modulus are listed in table 1.

4.2. Self-field I_c

Self-field I_c measurements were performed together with the stress-strain measurements (except for the YBCO/RABiTS#3 sample). Figures 4 and 5 show the data up to the highest applied stress, where an irreversible reduction of I_c was observed for the first time. The critical currents are normalized by the mean value (before the samples were irreversibly damaged) of the critical currents in the relaxed state and at zero field. (A small force of 10 N was applied also in the relaxed state in order to straighten the tape. Because of the different geometric cross sections of the tapes, this corresponds to a different pre-stress of 11 MPa in the YBCO/MOD tape and of 25 MPa in the GdBCO/IBAD tape.) The irreversible stress/strain limit was defined as the last value of applied stress/strain where I_c in the (following) relaxed state was above 95 % of the initial value.

4.2.1. YBCO/RABiTS The stress dependence of I_c in the YBCO/RABiTS conductor did not change significantly after irradiation (figure 4). However, it seems that a small maximum appears at around 100 MPa after irradiation. The pristine YBCO/RABiTS#1 sample was irreversibly damaged during the warm-up process after applying 303 MPa, therefore no data exist for higher stress values. Below
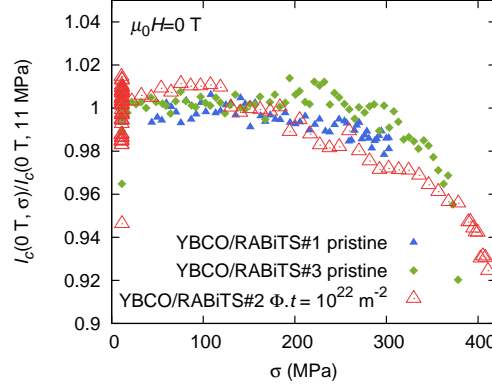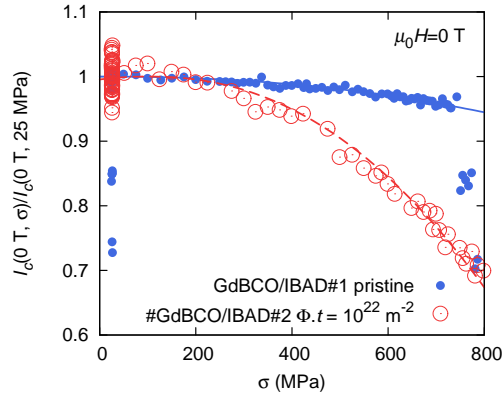
Figure 4. Self-field I_c dependence on stress (YBCO/RABiTS).

303 MPa ($\varepsilon \approx 0.33\%$), I_c was never reduced to below 98% of the original I_c. In the YBCO/RABiTS#3 sample, the irreversible stress limit was reached at 373 MPa ($\varepsilon \approx 0.46\%$). I_c of the irradiated sample was reduced to 92 % just below the irreversible stress limit of 410 MPa ($\varepsilon \approx 0.53\%$).

The relaxed I_c decreases after irradiation to 76% of I_c in the pristine sample. A T_c reduction of 1.8 K was measured in the reference sample. Furthermore, $B_{irr}(77\,K)$ was only slightly enhanced at this fluence.

4.2.2. GdBCO/IBAD Figure 5 shows the I_c-stress dependence of the GdBCO/IBAD sample.

Figure 5. Self-field I_c dependence on stress (GdBCO/IBAD).

After applying 740 MPa ($\varepsilon \approx 0.55\%$), the critical current was permanently reduced in the pristine sample. Two major reductions occurred between 740 MPa and 800 MPa. After the first reduction, I_c in the relaxed state was reduced to $\approx 83\%$ of its initial value. After applying 790 MPa, I_c in the relaxed state was reduced to $\approx 70\%$ of the initial value. Just below the irreversible stress limit of 740 MPa, I_c was reduced only by 5%. Note

Table 1. Summary of the parameters obtained from the self-field measurements. (T_c from reference samples)

Sample	σ_{irr}	ϵ_{irr}	T_c	I_c(0 T,relaxed)	n-value	$\overline{e}$
pristine YBCO#1	>303 MPa	>0.33 %	89.8 K	88.4 A	30.0	106 GPa
pristine YBCO#3	373 MPa	>0.46 %	89.8 K	93.6 A	30.7	115 GPa
irradiated YBCO#2	410 MPa	0.53 %	88.0 K	67.1 A	25.8	103 GPa
pristine GdBCO#1	740 MPa	0.55 %	92.9 K	142.7 A	33.2	163 GPa
irradiated GdBCO#2	800 MPa	0.65 %	86.7 K	16.52 A	18.2	139 GPa

that measurements of other samples from the same spool indicated irreversible stress limits of up to 800 MPa.

For the irradiated GdBCO/IBAD sample, the irreversible stress/strain limit was reached at 800 MPa/ε=0.65 %. I_c of the irradiated sample is more sensitive to applied stress than in the pristine sample. Close to the irreversible stress limit, I_c was reduced to 67% of the relaxed value.

The relaxed self-field I_c was reduced by one order of magnitude after irradiation. T_c in the reference sample was reduced by 6.2 K and also the irreversibility field significantly decreased at this temperature.

The lower T_c and the resulting higher T/T_c ratio of the irradiated tape at 77 K seem to be responsible for the change of the I_c-sensitivity to applied stress. A higher I_c-sensitivity at temperatures closer to T_c was found for YBCO tapes in Ref. [10] and is expected from the equation for a single grain [25]:

$$I_{c,sg}(T,\sigma,b) = I_c(T=0,\sigma=0)\left(1-\frac{T}{b\,\sigma+T_c(0)}\right)^{1.5} \qquad (1)$$

where $T_c(0)$ is the critical temperature at zero applied strain and b denotes the change of T_c with applied pressure. The anisotropic pressure dependence of b was found to be b_a=-2.0±0.2 K/GPa and b_b=1.9±0.2 K/GPa with pressure along the a-axis and the b-axis, respectively [14]. For small σ equation 1 leads to first order to

$$I_c(\sigma)/I_c(0) = 1 - 1.5\frac{bT}{T_c(T_c-T)}\sigma + o(\sigma^2). \qquad (2)$$

The strain sensitivity thus increases with decreasing transition temperature, in particular, if T_c approaches T, as in the irradiated GdBCO/IBAD sample. Note that a pronounced curvature in $I_c(\sigma)$ is observed experimentally instead of the predicted linear behavior. This is a consequence of the dependence of the critical currents on the applied electric field. A model with two grains oriented with their a-axis parallel and perpendicular to the tape direction was presented in [25], which describes the stress dependence of I_c in YBCO coated conductors qualitatively. However, since a real coated conductor is a percolative network of differently aligned grains, a quantitative model needs to be developed for a comparison with experimental data.

4.3. Homogeneity

Figure 6 shows magnetoscan images of the pristine GdBCO sample before and after the tensile stress measurements. The virgin conductor (figure 6a) is very homogeneous
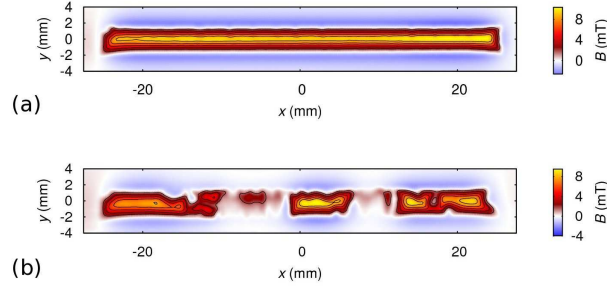
Figure 6. Magnetoscan images of the pristine GdBCO#1 sample before (a) and after (b) applying a tensile load of 320 MPa.

without significant defects. The conductor was irreversibly damaged after applying the maximum load of 740 MPa. After removing the sample from the set-up, no destruction was found by optical inspection. The magnetoscan image (figure 6b) reveals the degree of damage. The superconducting layer was damaged over a long length and not only along single distinctive macroscopic cracks. The two main defects around $x = -5$ mm and $x = 10$ mm may correlate with the two significant reductions of I_c at $\approx$740 MPa and $\approx$800 MPa presented in figure 5.

Note that the left and right ends, where the current clamps held the sample, are less damaged. Hence, the pressure exerted by the current terminals does not destroy the sample and a good current feed is ensured.

4.4. In-field I_c anisotropy

The angular dependence of I_c at liquid nitrogen temperature changes completely after irradiation in both samples.

In the YBCO/RABiTS conductor the strong additional pinning centres introduced by fast neutron irradiation lead to an enhancement of I_c between the two a,b peaks.

Figure 7‡ shows the dependence of I_c in the pristine YBCO/RABiTS sample on the applied stress at $\mu_0 H$=1.4 T.

The two maxima of I_c occur for fields parallel to the a,b-planes and the I_c-anisotropy (ratio of $I_c(H\|a,b)/I_c(H\|c)$) is quite low. As expected from the self-field measurements, the applied stress hardly influences the critical current up to the maximum applied stress of 303 MPa. For lower fields (not shown), the anisotropy is even smaller and no significant influence of applied stress was found either.

‡ Note that the color code in all following 3D-figures refers to a normalization of I_c by the (right) maximum near $H\|$a,b (at 90° and around 85° in the YBCO/RABiTS and GdBCO/IBAD tape, respectively. 0° refers to the field parallel to the c-axis.)
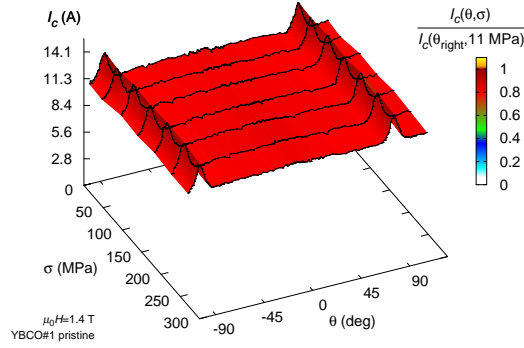
Figure 7. Critical current anisotropy of the pristine YBCO/RABiTS sample at $\mu_0 H = 1.4$ T.

As already discussed, I_c of the YBCO/RABiTS tape is enhanced by the irradiation between the a,b-peaks (figure 8). The a,b-peaks on the other hand are reduced. No stress
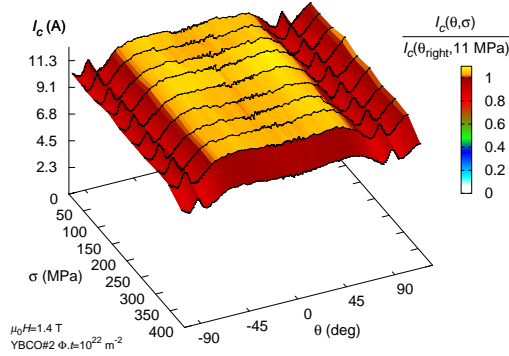
Figure 8. Critical current anisotropy of the irradiated YBCO/RABiTS sample at $\mu_0 H = 1.4$ T.

dependence of the in-field I_c in the irradiated sample was found within experimental accuracy up to the second highest applied stress of 346 MPa, but a reversible degradation to 90% of the initial I_c occurs at 389 MPa. Furthermore, no field dependence of the stress-sensitivity was observed up to 346 MPa for all orientations. Figure 9 shows the I_c-dependence on the tensile stress at various fields ($H \| c$). At the highest applied stress of 389 MPa, the degradation is higher at higher fields. This effect is less pronounced at $H \| a,b$(not shown).

Contrary to the YBCO/RABiTS tape, I_c of the pristine sample is asymmetric with respect to the c-axis in the GdBCO/IBAD conductor. At 0.1 T, the peaks are shifted by -11° (Θ_{left}) and -6.5° (Θ_{right}) respectively with respect to the tape surface. With increasing field the shift is reduced to about -4°at 1.4 T for both peaks. Furthermore,
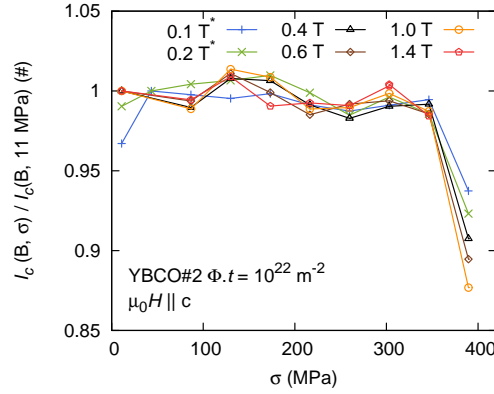
**Figure 9.** Stress dependence of I_c of the irradiated YBCO/RABiTS sample for different fields $H\|$c. Note that the 0.1 T and 0.2 T values are normalized by the values at 44 MPa as the temperature was too high at 0.11 MPa.

I_c at Θ_{right} is always higher than at Θ_{left}. A more detailed description of the angular dependence in similar tapes can be found elsewhere [26, 27, 28]. The applied tensile stress neither influences the angular dependence of I_c nor the positions of the local maxima.

Note that a reduction of the peak shift from 12° towards 0° as well as a change of the angular I_c-dependence were observed under *compressive* strain at 0.5 T in Ref. [8] in an YBCO/IBAD sample.

Figure 10 shows the angular and stress dependence of I_c in the pristine sample at μ_0H=0.6 T. Θ_{left} corresponds to the local peak at around -95°, Θ_{right} to the local peak at around 85°. A local minimum occurs at around -30°. As in the self-field measurements,
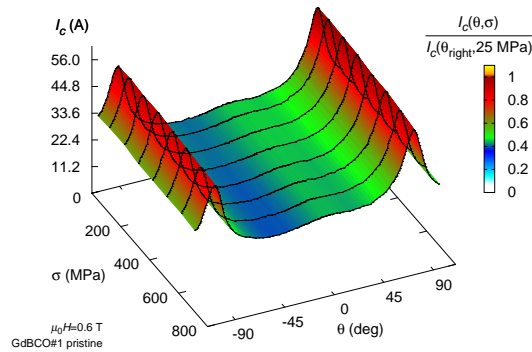
Figure 10. Critical current anisotropy of the pristine GdBCO/IBAD sample at μ_0H=0.6 T.

the critical current does not significantly change with the applied stress in the reversible region. The field and stress dependence on the normalized I_c for $H\|$c is shown in figure 11 for the pristine sample. The reduction of I_c is weaker at 0.4 T, especially
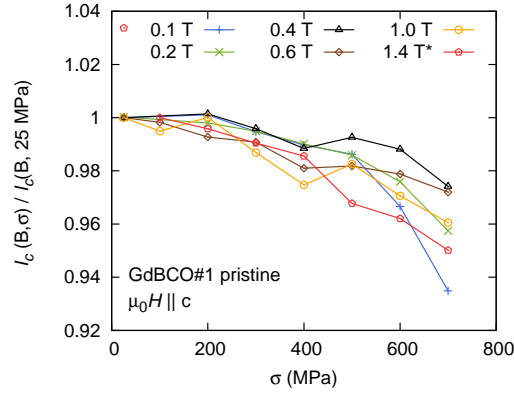
Figure 11. Stress dependence of I_c for $H \| c$ of the pristine GdBCO/IBAD sample at different fields. At 25 MPa/1.4 T the temperature was too high. Therefore, I_c of the 1.4 T measurement was normalized by I_c at 100 MPa

at higher applied stress. A weaker stress sensitivity of I_c in YBCO/IBAD samples at around $\mu_0 H$=0.2 T-0.25 T was also found in [10][5]. This field dependence of the stress sensitivity is accompanied by a shift of the maximum I_c from zero to finite strain in YBCO/IBAD samples [5][10], which is not observed in the GdBCO/IBAD samples.

For $H \| \Theta_{right}$ I_c decreases monotonously with increasing field (not shown) like in the YBCO/MOD sample, but the reduction starts already at lower applied stress.

After irradiation, the angular dependence of I_c becomes more symmetric with respect to the c-axis and both maxima are located approximately -7° off the tape surface at 0.1 T. The maxima shift with field and converge at -4° at 1.4 T. The reduction of I_c by stress is significantly higher over the entire angular range compared to the pristine sample.

Figure 12 shows the angular and stress dependence of I_c at 0.6 T. A clear maximum
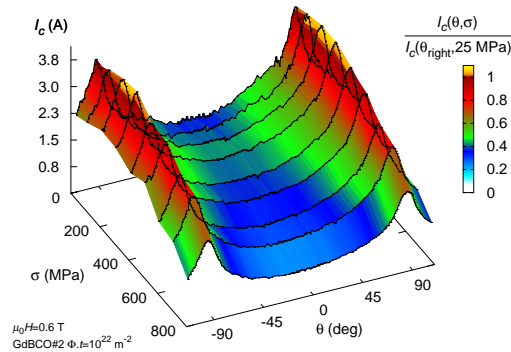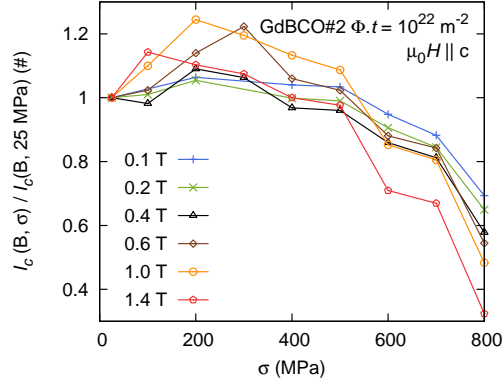

Figure 12. Critical current anisotropy of the irradiated GdBCO/IBAD sample at $\mu_0 H$=0.6 T.

at around 200 MPa occurs over the entire angular range. The minimum of I_c is found

at around $H \| c$ independently of stress.

The field and stress dependent change of I_c at $H \| c$ is illustrated in figure 13. The

Figure 13. Stress dependence of I_c for $H \| c$ of the irradiated GdBCO sample for different fields.

critical current reaches a maximum at an applied stress of 200 -300 MPa. At intermediate fields (0.6 T and 1.0 T), significantly higher values of I_c are reached at 200 MPa. On the other hand, at higher applied stress, the reduction of the critical currents increases monotonously with field.

At $H \| \Theta_{right}$ the maximum of I_c at around 200 MPa was not as pronounced as for $H \| c$, but still visible. At high applied stress, I_c is once again more strongly reduced at higher applied field.

5. Conclusion

Measurements of the critical currents under tensile stress in pristine and neutron irradiated YBCO/MOD and GdBCO/IBAD coated conductors were performed in magnetic fields of up to 1.4 T. The field orientation varied within a range of about 220° including both a,b-peaks ($H \| a,b$).

The critical currents in GdBCO/IBAD were significantly reduced after irradiation due to the strong reduction of T_c by 6.2 K. Thermal and epi-thermal neutrons captured by the ^{155}Gd and ^{157}Gd-nuclei seem to be responsible for this strong reduction, as the recoil energy during gamma emission introduces additional point defects. These point defects are responsible for enhanced disorder. Thermal neutron absorption does not play a role in YBCO because the neutron absorption cross sections are too small for all constituents of YBCO.

The irreversible stress/strain limit of the GdBCO/IBAD and the YBCO/MOD sample do not change significantly after irradiation. The stress dependence of I_c in YBCO/MOD did not change after irradiation, whereas the sensitivity of I_c to stress was significantly enhanced in GdBCO/IBAD. This change can be ascribed to the lower

T_c and the resulting higher ratio of T/T_c at liquid nitrogen temperature. At the highest applied field (1.4 T), I_c at 800 MPa was reduced to less than 40% of the relaxed I_c-value.

Further experiments, where the thermal neutrons are shielded during the irradiation, have to complement the existing data to judge the possible application of GdBCO conductors in future fusion devices.

Acknowledgments

References

[1] T. G. Holesinger, L. Civale, B. Maiorov, D. M. Feldmann, J. Y. Coulter, D. J. Miller, V. A. Maroni, Z. Chen, D. C. Larbalestier, R. Feenstra, X. Li, Y. Huang, T. Kodenkandath, W. Zhang, M. W. Rupich, and A. P. Malozemoff. Progress in nanoengineered microstructures for tunable high-current, high-temperature superconducting wires. *Advanced Materials*, 20(3):391–407, 2008.

[2] Martin W Rupich, Xiaoping Li, Cees Thieme, Srivatsan Sathyamurthy, Steven Fleshler, David Tucker, Elliot Thompson, Jeff Schreiber, Joseph Lynch, David Buczek, Ken DeMoranville, James Inch, Paul Cedrone, and James Slack. Advances in second generation high temperature superconducting wire manufacturing and R&D at American Superconductor Corporation. *Superconductor Science and Technology*, 23(1):014015, 2010.

[3] V. Selvamanickam, Yimin Chen, Xuming Xiong, Y.Y. Xie, M. Martchevski, A. Rar, Yunfei Qiao, R.M. Schmidt, A. Knoll, K.P. Lenseth, and C.S. Weber. High Performance 2G Wires: From R&D to Pilot-Scale Manufacturing. *IEEE Transactions on Applied Superconductivity*, 19(3):3225 –3230, 2009.

[4] D. C. Van Der Laan, J. F. Douglas, L. F. Goodrich, R. Semerad, and M. Bauer. Correlation between in-plane grain orientation and the reversible strain effect on flux pinning in RE-Ba$_2$Cu$_3$O$_{7-\delta}$ coated conductors. *IEEE Transactions on Applied Superconductivity*, 22(1):8400707, 2012.

[5] D. C. Van Der Laan, J. W. Ekin, J. F. Douglas, C. C. Clickner, T. C. Stauffer, and L. F. Goodrich. Effect of strain, magnetic field and field angle on the critical current density of YBa$_2$Cu$_3$O$_{7-\delta}$ coated conductors. *Superconductor Science and Technology*, 23(7):072001, 2010.

[6] N. Cheggour, J.W. Ekin, and C.L.H. Thieme. Magnetic-field dependence of the reversible axial-strain effect in Y-Ba-Cu-O coated conductors. *IEEE Transactions on Applied Superconductivity*, 15(2):3577–3580, 2005.

[7] D. Uglietti, B. Seeber, V. Abcherli, W. L. Carter, and R. Flkiger. Critical currents versus applied strain for industrial Y-123 coated conductors at various temperatures and magnetic fields up to 19 T. *Superconductor Science and Technology*, 19(8):869–872, 2006.

[8] J.S. Higgins and D.P. Hampshire. Critical Current Density of YBa$_2$Cu$_3$O$_{7-\delta}$ Coated Conductors Under High Compression in High Fields. *Applied Superconductivity, IEEE Transactions on*, 21(3):3234 –3237, June 2011.

[9] Kozo Osamura, Michinaka Sugano, Kohichi Nakao, Yuh Shiohara, Akira Ibi, Yutaka Yamada, Naoji Nakashima, Shigeo Nagaya, Takashi Saitoh, Yasuhiro Iijima, Yuhji Aoki, Takayo Hasegawa, and Takeshi Kato. Reversible strain limit of critical currents and universality of intrinsic strain effect for REBCO-coated conductors. *Superconductor Science and Technology*, 22(2):025015 (7pp), 2009.

[10] M. Sugano, T. Nakamura, T. Manabe, K. Shikimachi, N. Hirano, and S. Nagaya. The intrinsic strain effect on critical current under a magnetic field parallel to the c axis for a MOCVD-YBCO-coated conductor. *Superconductor Science and Technology*, 21(11):115019 (8pp), 2008.

[11] M. Eisterer, R. Fuger, M. Chudy, F. Hengstberger, and H. W. Weber. Neutron irradiation of coated conductors. *Superconductor Science and Technology*, 23(1):014009, 2010.

[12] R. Fuger, M. Eisterer, and H. W. Weber. YBCO coated conductors for fusion magnets. *IEEE Transactions on Applied Superconductivity*, 19(3):1532–1535, 2009.

[13] D. C. Van der Laan, J. F. Douglas, C. C. Clickner, T. C. Stauffer, L. F. Goodrich, and H. J. N. Van Eck. Evidence that the reversible strain effect on critical current density and flux pinning in Bi$_2$Sr$_2$Ca$_2$Cu$_3$O$_x$ tapes is caused entirely by the pressure dependence of the critical temperature. *Superconductor Science and Technology*, 24(3):032001, 2011.

[14] U. Welp, M. Grimsditch, S. Fleshler, W. Nessler, J. Downey, G. W. Crabtree, and J. Guimpel. Effect of uniaxial stress on the superconducting transition in YBa$_2$Cu$_3$O$_7$. *Physical Review Letters*, 69(14):2130–2133, 1992.

[15] M. C. Frischherz, M. A. Kirk, J. Farmer, L. R. Greenwood, and H. W. Weber. Defect cascades produced by neutron irradiation in YBa$_2$Cu$_3$O$_{7-\delta}$. *Physica C: Superconductivity*, 232:309 – 327, 1994.

[16] M. Aleksa, P. Pongratz, O. Eibl, F.M. Sauerzopf, H.W. Weber, T.W. Li, and P.H. Kes. TEM observation of neutron-induced collision cascades in Bi-2212 single crystals. *Physica C: Superconductivity*, 297(34):171 – 175, 1998.

[17] K. E. Sickafus, J. O. Willis, P. J. Kung, W. B. Wilson, D. M. Parkin, M. P. Maley, F. W. Clinard, C. J. Salgado, R. P. Dye, and K. M. Hubbard. Neutron-radiation-induced flux pinning in Gd-doped YBa$_2$Cu$_3$O$_{7-x}$ and GdBa$_2$Cu$_3$O$_{7-x}$. *Physical Review B*, 46:11862–11870, Nov 1992.

[18] M. Chudý, M. Eisterer, H. W. Weber, J. Veterníková, S. Sojak, and V. Slugeň. Point defects in YBa$_2$Cu$_3$O$_{7-x}$ studied using positron annihilation. *Superconductor Science and Technology*, 25(7):075017, 2012.

[19] National Nuclear Data Center, Brookhaven National Laboratory ENDF/B-VII.1 library.

[20] H.W. Weber, H. Böck, E. Unfried, and L.R. Greenwood. Neutron dosimetry and damage calculations for the TRIGA MARK-II reactor in Vienna. *Journal of Nuclear Materials*, 137(3):236 – 240, 1986.

[21] F. M. Sauerzopf. Anisotropic flux pinning in YBa$_2$Cu$_3$O$_{7-\delta}$ single crystals: The influence of defect size and density as determined from neutron irradiation. *Physical Review B*, 57:10959–10971, May 1998.

[22] M Eisterer, S Haindl, T Wojcik, and H W Weber. 'Magnetoscan': a modified Hall probe scanning technique for the detection of inhomogeneities in bulk high temperature superconductors. *Superconductor Science and Technology*, 16(11):1282, 2003.

[23] M. Zehetmayer, R. Fuger, M. Eisterer, F. Hengstberger, and H. W. Weber. Assessment of the local supercurrent densities in long superconducting coated conductors. *Applied Physics Letters*, 90(3):032506, 2007.

[24] Jack W. Ekin. *Experimental Techinques for Low Temperature Measurements*. Oxford University Press, 2006.

[25] D. C. Van Der Laan, D. Abraimov, A. A. Polyanskii, D. C. Larbalestier, J. F. Douglas, R. Semerad, and M. Bauer. Anisotropic in-plane reversible strain effect in Y$_{0.5}$Gd$_{0.5}$Ba$_2$Cu$_3$O$_{7-\delta}$ coated

conductors. *Superconductor Science and Technology*, 24(11):115010, 2011.

[26] B. Maiorov, B. J. Gibbons, S. Kreiskott, V. Matias, T. G. Holesinger, and L. Civale. Effect of the misalignment between the applied and internal magnetic fields on the critical currents of tilted coated conductors. *Applied Physics Letters*, 86:13204, 2005.

[27] Y. Chen, V. Selvamanickam, Y. Zhang, Y. Zuev, C. Cantoni, E. Specht, M. P. Paranthaman, T. Aytug, A. Goyal, and D. Lee. Enhanced flux pinning by $BaZrO_3$ and $(Gd,Y)_2O_3$ nanostructures in metal organic chemical vapor deposited GdYBCO high temperature superconductor tapes. *Applied Physics Letters*, 94:062513, 2009.

[28] Chudý M., S. C. Hopkins, M. Woźniak, Glowacki B. A., Eisterer M., and H. W. Weber. Full angular critical current characteristics of coated conductors studied using a two-axis high current goniometer. *Superconductor Science and Technology*, 24(7):075018, 2011.